Synthesis of Ternary Metal Nitride Nanoparticles Using Mesoporous Carbon Nitride as Reactive Template

Anna Fischer,[†] Jens Oliver Müller,[‡] Markus Antonietti,[†] and Arne Thomas[†,*]

[†]Max Planck Institute of Colloids and Interfaces, Research Campus Golm, Am Muehlenberg 1, D-14476 Golm, Germany, and [‡]Fritz-Haber-Institute of the Max-Planck-Society, Department of Inorganic Chemistry, Faradayweg 4-6, D-14195 Berlin, Germany

ABSTRACT Mesoporous graphitic carbon nitride was used as both a nanoreactor and a reactant for the synthesis of ternary metal nitride nanoparticles. By infiltration of a mixture of two metal precursors into mesoporous carbon nitride, the pores act first as a nanoconfinement, generating amorphous mixed oxide nanoparticles. During heating and decomposition, the carbon nitride second acts as reactant or, more precisely, as a nitrogen source, which converts the preformed mixed oxide nanoparticles into the corresponding nitride (reactive templating). Using this approach, ternary metal nitride particles with diameters smaller 10 nm composed of aluminum gallium nitride (Al—Ga—N) and titanium vanadium nitride (Ti—V—N) were synthesized. Due to the confinement effect of the carbon nitride matrix, the composition of the resulting metal nitride can be easily adjusted by changing the concentration of the preceding precursor solution. Thus, ternary metal nitride nanoparticles with continuously adjustable metal composition can be produced.

KEYWORDS: nanoparticles · template · carbon nitride · metal nitride · mesoporous · semiconductor · catalysis

Metal nitrides have attracted growing interest in recent years as their properties can complement metal oxides in a variety of applications. Thus, metal nitrides exhibit enhanced hardness and are therefore applied as abrasive materials.[1] The metal nitrides formed from group III metals are wide band gap semiconductors and can be used as optoelectronic materials.[2] Furthermore, the applications of metal nitrides as electrodes for supercapacitors[3] or as catalyst[4−8] were reported. Especially for the latter applications, the control of the nanostructure of the metal nitride and naturally its composition can have a crucial influence on its overall performance. In this respect, the formation of ternary metal nitrides, that is, of metal nitrides featuring two metals in their crystal structure, can widely expand the properties of this class of materials. This is especially obvious for the application of metal nitrides as semiconductors. The band gap of pure binary metal nitrides features values of 0.7 eV for indium nitride (InN), 3.4 eV for gallium nitride (GaN), and 6.3 eV for aluminum nitride (AlN), respectively, and thus can be used for violet, blue, and green light emitting devices.[9] It is certainly appealing to mix such metal nitrides into ternary metal nitrides, as for example an Al−Ga−N alloy with different compositions will allow one to adjust the size of the band gap continuously between the values of the pure metal nitrides.[10]

Titanium vanadium nitride (Ti−V−N) coatings represent another example for the superior performance of ternary metal nitrides, as they show excellent hardness and friction properties compared to pure titanium nitride (TiN) or vanadium nitride (VN) coatings.[11,12] Moreover, small amounts of vanadium in a titanium nitride should stabilize this material in applications such as electrodes for supercapacitors.[13] These examples show that a general and facile approach, combining control over composition *and* nanostructure of ternary nitrides in one step, would be certainly beneficial.

In general, ternary metal nitrides can be prepared by heating the respective ternary oxide precursor with nitrogen donors such as ammonia or urea.[14−16] Also, solid state metathesis reactions using for example Li_3N or NaN_3 have been reported.[17−21] However, the synthesis of defined nanostructured ternary metal nitrides is so far just rarely described (except for ternary III nitrides, especially InGaN, where several nanostructures were reported using vapor deposition[22−24] or precursor route[25,26] techniques).

The synthesis of a high surface area V−Mo−N powder was achieved using nitridation of amine intercalated ternary oxide foams in a high temperature ammonia flow.[27]

Herein we report on the synthesis of ternary metal nitride nanoparticles using a

*Address correspondence to arne.thomas@mpikg.mpg.de.

Received for review August 7, 2008 and accepted October 21, 2008.

Published online November 12, 2008.
10.1021/nn800503a CCC: $40.75

"reactive hard templating" approach, exemplified by the synthesis of Al−Ga−N and Ti−V−N nanoparticles. "Hard templating", using mainly inorganic nanostructures as endo- or exotemplate,[28] is widely applied for the synthesis of mesoporous polymers, carbon nitrides, and carbon materials.[29,30] After removal of the hard template, the resulting material is often in fact an inverse replica of the initial template. Consequently, repeated hard templating procedures,[31] including two successive replications steps, yield in direct copies, exhibiting ideally a similar nanostructure as observed in the initially used template. In the approach presented here, termed reactive templating, the template acts additionally as reactant, thus determining not only the structure but also the chemical composition of the resulting material. Recently, we reported on the synthesis of binary metal nitride nanoparticles using such a reactive templating.[32] A mesoporous carbon nitride synthesized with silica nanoparticles as template[33] were first used as exotemplate for the preparation of metal oxide nanoparticles and then as a nitrogen source converting the metal oxides into the corresponding nitride.

Herein we show that ternary metal nitride nanoparticles can be synthesized using mesoporous carbon nitrides as reactive hard template accordingly. Thus, a variety of nanostructured ternary nitrides (here Al−Ga−N and V−Ti−N) can be produced with the possibility to continuously tune the metal ratios in their composition.

RESULTS AND DISCUSSION

Mesoporous graphitic carbon nitride (mpg-C_3N_4), was synthesized as already described.[33] Elemental analysis of the resulting material is proving a composition close to the ideal stochiometry. From X-ray measurements (Figure S1 in the Supporting Information), a graphitic stacking in the material can be observed, indicated by a peak at 27.5°, which can be indexed according to the (002) peak from a graphitic structure while the peak at 13.1° can be attributed to an in-plane periodic order.[34] The mpg-C_3N_4 used in this study as reactive template features interconnected 12 nm spherical pores and a surface area of 220 m^2/g proven by TEM, SAXS, and nitrogen sorption measurements (Figure S2−S4 in the Supporting Information), respectively.

TABLE 1. Composition of the Infiltrating Solutions for the Synthesis of Al−Ga−N and Ti−V−N Nanoparticles in mpg-C_3N_4 (Numbers Describe the Molar Ratio of the Metals in the Initial Precursor Solutions)

sample	$AlCl_3$ (mg)	$GaCl_3$ (mg)	EtOH (g)	Al/Ga mol ratio
AlGaN-0.20	110.0	730.0	2.0	0.20
AlGaN-0.72	290.0	530.0	2.0	0.72
AlGaN-1.46	400.0	360.0	2.0	1.46
sample	$VOCl_3$ (mg)	$TiCl_4$ (mg)	EtOH (g)	V/Ti mol ratio
TiVN-0.19	170.0	1000.0	2.0	0.19
TiVN-0.55	400.0	800.0	2.0	0.55
TiVN-1.46	800.0	600.0	2.0	1.46

The synthesis of two series of ternary metal nitrides were studied, first aluminum/gallium nitrides and second titanium/vanadium nitrides. Similar synthesis routes were applied for the synthesis of nanoparticles from these precursors: Three precursor solutions with different concentrations of $GaCl_3$ and $AlCl_3$ or $TiCl_4$ and $VOCl_3$, respectively, were prepared in ethanol, and the nanoreactor (mpg-C_3N_4) was added to these solutions (Table 1). The infiltrated powder was collected and carefully washed with 2 mL EtOH during suction filtration, ensuring that the precursor solutions are located in the pores of the nanoreactor only. During drying of the carbon nitride/precursor composite, the formation of amorphous mixed oxide nanoparticles confined in the mesopores can be assumed. It has been shown that heating of these composites in the case of pure metal precursors yields the formation of binary metal nitride nanoparticles, by donating nitrogen atoms from the carbon nitride nanoreactor to the preformed metal oxide nanoparticles.[32]

The same mechanism can be assumed for precursor mixtures confined in the mesopores of mpg-C_3N_4, with the advantage that a possible demixing or phase separation of the different metals is prevented as long as the nanoconfinement is present. In the following, the synthesis of aluminum gallium nitrides and titanium vanadium nitrides are discussed separately.

Synthesis of Al−Ga−N Nanoparticles in Mesoporous Graphitic Carbon Nitride. Solutions of $AlCl_3$ and $GaCl_3$ in ethanol with different Al/Ga molar ratios were used as precursors and infiltrated into mpg-C_3N_4 (see Table 1). To define the boundary cases, pure $AlCl_3$ and $GaCl_3$ solutions were used, which yield in the formation of the pure, binary nitrides. The infiltrated mpg-C_3N_4 powders were heated to 800 °C under nitrogen flow, as described for the synthesis of pure GaN nanoparticles.[32] It should be noted that the reaction can be also carried out under argon

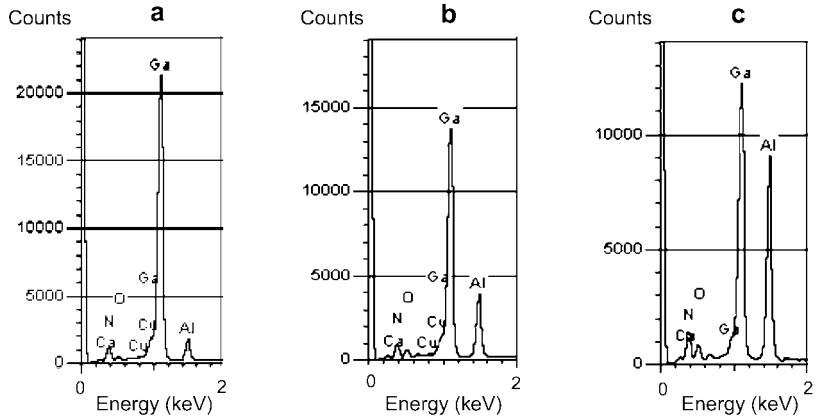

Figure 1. EDX measurements of the Al−Ga−N nanoparticles: (a) AlGaN-0.20, (b) AlGaN-0.72, and (c) AlGaN-1.46.

TABLE 2. Composition of the Different Al−Ga−N Nanocrystalline Powders Determined by EDX (Al,Ga, O) and Elemental Analysis (N,C): For Comparison, the Initial Molar Ratios of the Metals in the Precursor Solution Are Also Shown

sample	Al wt %	Ga wt %	N wt %	C wt %	O wt %	residue wt %	molar ratio Al/Ga (powder)	molar ratioAl/Ga (solution)
AlGaN-0.20	6.41	73.81	15.28	0.00	0.76	3.74	0.22	0.20
AlGaN-0.72	19.20	62.46	15.17	0.00	1.20	1.83	0.79	0.72
AlGaN-1.46	28.68	52.03	15.02	0.00	0.88	3.39	1.42	1.46

or in sealed quartz ampoules, proving that the nitrogen is provided by the C_3N_4 template. A higher temperature than the decomposition temperature of mpg-C_3N_4 (~650 °C) was used, as this temperature should ensure complete removal of the template. After the samples were completely cooled to room temperature under nitrogen atmosphere, powders from light yellow-brown to light gray in color were obtained (with increasing amount of aluminum). The composition of the powders was determined using electron dispersive X-ray spectroscopy (EDX) and elemental analysis. The EDX measurements in Figure 1 illustrate the increasing aluminum content of the resulting powders, following the increasing amount of aluminum in the preceding precursor mixtures. Table 2 summarizes the composition of the powders determined by EDX. It can be seen that the molar ratios of the initial precursor solutions are nearly perfectly reflected in the resulting metal nitrides. The nitrogen content of the samples was additionally confirmed by elemental analysis. For all three samples, the amount of nitrogen found is approximately 15 wt %, which is in good agreement with the EDX determined values. Only traces of oxygen could be detected, indicating that only minor surface oxidation on the nanoparticles occurs. Remarkably, no carbon contamination is found in the powders, which is confirmed both by EA and EDX.

Powder X-ray diffraction measurements (PXRD) (Figure 2) show that all powders feature hexagonal symmetry and crystallize in the space group *P*63*mc*, according to a solid solution of GaN and AlN. Comparing these patterns with the reflections found for pure gallium and aluminum nitride, a significant shift in the pattern of the powders from lower angles, that is, from pure GaN, to higher angles toward pure AlN is observed with increasing aluminum content in the powders (Figure 2). This shift indicates the formation of a solid solution, thus aluminum atoms progressively substitute gallium atoms in the crystal. The cell parameters for each sample and those of pure GaN and AlN are listed in Table 3.

The Scherrer equation was applied to the (102) and the (110) peaks to determine an average crystal size for each sample. The most intensive peak, namely, the (101) peak, could not be used to determine the crystallite size since it overlaps with the adjacent (002) peak. With increasing aluminum content, a decrease in the crystal size from 9.6 to 5.9 nm is observed in the ternary samples, while the binary metal nitrides show a similar crystallite size of approximately 9 nm. However, it should be noted that, although the broadness of the reflection peaks is related to the crystal size, also the quality of the crystal structure can have a significant influence.[35] Thus, progressive peak broadening could also reflect a loss in crystallinity due to an increasing number of defects when the aluminum content is increased. However, in the

TABLE 3. Cell Parameters and Crystallite Size of the Observed Al−Ga−N, GaN, and AlN Powders Synthesized in the Same Reaction Conditions

	cell parameter [Å] *P*63*mc*			
sample	a	c	cryst size XRD	particle size TEM
GaN	3.189	5.184	9.1	9.0
AlGaN-0.20	3.179	5.16	9.6	9.2
AlGaN-0.72	3.173	5.138	7.5	7.4
AlGaN-1.46	3.165	5.105	5.9	4.2
AlN	3.112	4.975	9.5	11

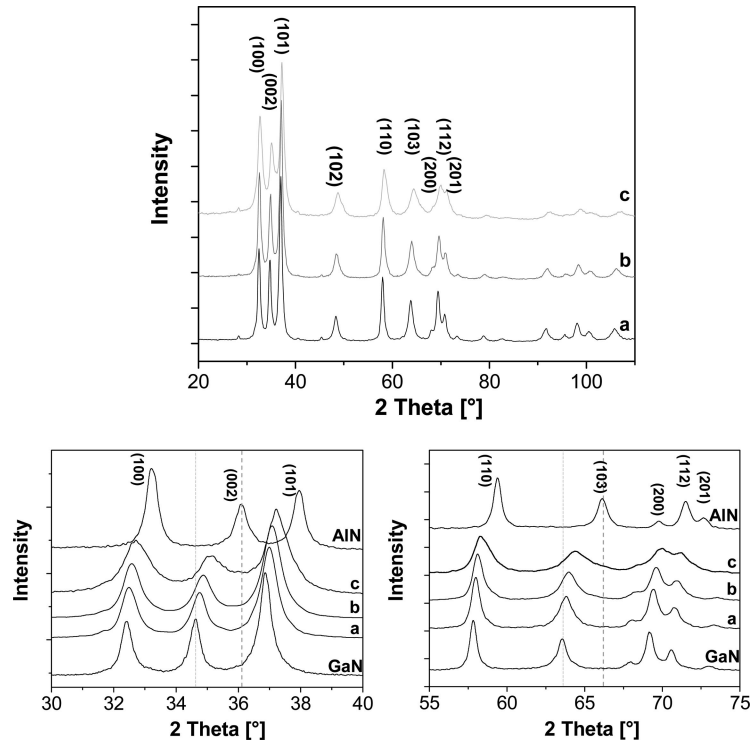

Figure 2. Powder X-ray diffraction pattern of the Al−Ga−N nanocrystalline powders with increasing aluminum content: (a) AlGaN-0.20, (b) AlGaN-0.72, and (c) AlGaN-1.46. As a reference, the patterns of pure GaN and AlN synthesized in the same conditions are also shown.

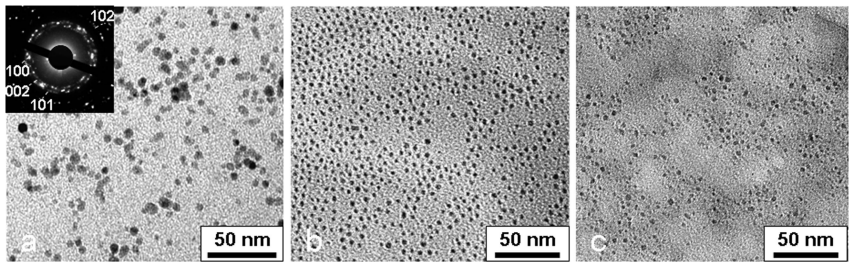

Figure 3. TEM micrographs of the Al−Ga−N samples: (a) AlGaN-0.20, (b) AlGaN-0.72, and (c) AlGaN-1.46. The powders were dispersed in THF using oleic acid prior to the measurements.

case of the AlGaN-1.46 sample, a small shoulder at higher angles is present in the (102) peak. Thus, it is likely that a component with a higher Al content, and thus smaller lattice parameters (shoulder), coexists with the major phase (main (102) peak).

The size and shape of the particles were investigated by transmission electron microscopy (TEM). The TEM measurements (Figure 3) of dispersed samples show that the powders consist of small nanoparticles with a narrow dispersity, confirming the results obtained from the X-ray diffraction and supporting the concept that nanoparticles are formed through the confinement by the mesopores of the carbon nitride. The average particle size determined from the TEM pictures (see Table 2) correlates with small deviations with the crystallite size determined from the Scherrer equation.

The particle sizes derived from XRD and TEM are smaller than the pore size of the initial template, mpg-C_3N_4, which features a pore of 12 nm in diameter. This can also be expected as the metal precursors are introduced as solutions in the nanoconfinement, thus they are not able to completely fill out the pore. In a recent paper, it has been shown that indeed the concentration of the precursor solution can be used to tune the size of the resulting nanoparticles.[32]

In Figure 4, a complementary HRTEM measurement is shown. The powders consist of highly crystalline, agglomerated nanoparticles, as depicted by the presence

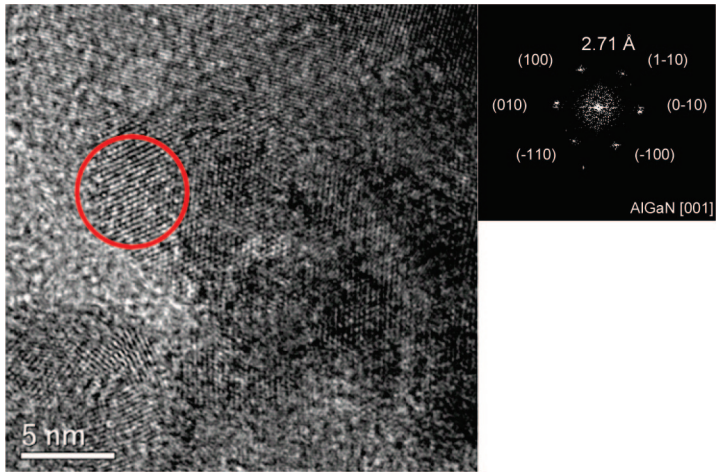

Figure 4. HRTEM micrograph of the sample AlGaN-1.46. The inset shows the indexed FFT of the area delimited with the red circle.

of well-developed lattice fringes. To ensure an accurate comparison between the lattice distances in the three samples, just particles oriented along the [001] zone axis were chosen for measurements. The measured lattice distances for the samples AlGaN-0.20, AlGaN-0.72, and AlGaN-1.46 were 2.74, 2.73, and 2.71 Å, respectively (Figure S5 in the Supporting Information). These distances do not perfectly fit with the d_{100} lattice distances measured by XRD (Table 2) but at least follow the observed trend, namely, that the lattice distances decrease with increasing aluminum content. This confirms on the nanometer scale the formation of an Al−Ga−N solid solution in the form of nanoparticles, formed from the preceding mixed solutions confined in the mesopores of the nitrogen donor, namely, mpg-C_3N_4.

It can be concluded that mesoporous carbon nitride is indeed a suitable nanoreactor for the synthesis of pure Al−Ga−N nanoparticles with dimensions less than 10 nm. Furthermore, it was shown that the composition of the alloy nanoparticles could be continuously adjusted in the experimental range explored here by simply changing the Al/Ga ratio in the precursor solution.

Synthesis of Ti−V−N Nanoparticles in Mesoporous Graphitic Carbon Nitride. To prove the versatility of the approach shown here, the concept was expanded to the preparation of nanoparticles from a second ternary metal nitride, namely, titanium vanadium nitride. Here, solutions of $TiCl_4$ and $VOCl_3$ in ethanol with different Ti/V molar ratios were used as precursors and infiltrated into mpg-C_3N_4 (see Table 1). Pure $TiCl_4$ or $VOCl_3$ solutions were used to prepare also the pure binary metal nitrides as boundary cases. The infiltrated mpg-C_3N_4 powders were heated to 800 °C under nitrogen flow, as described for the synthesis of pure TiN or VN nanoparticles.[32] After the samples were completely cooled to room temperature under nitrogen atmosphere, black powders were observed in all cases.

The composition of the powders was investigated as described for Al−Ga−N nanoparticles. The EDX (Figure 5) measurements of the powders show the increasing vanadium content following the concentrations in the preceding precursor solution.

However, contrary to the Al−Ga−N nanoparticles where no residual carbon was observed, for Ti−V−N samples, large amounts of carbon are detected (Table 4). This is not surprising since similar observations were made for mesoporous TiN[8] and TiN nanoparticles[36] synthesized with carbon nitride (or cyanamide) as nitrogen source. Furthermore, the amount of oxygen found in the samples is higher than in the case of the $Al_xGa_{1-x}N$ samples, thus some amount of surface oxidation has to be taken into account. Nevertheless, the

TABLE 4. Composition Determined by EDX (Ti,V, O) and Elemental Analysis (C,N) of the Different Ti−V−N Powders: For Comparison, the Initial Molar Ratios of the Metals in the Precursor Solution Are Also Shown

sample	V wt %	Ti wt %	N wt %	C wt %	O wt %	residue wt %	molar ratio V/Ti (powder)	molar ratio V/Ti (solution)
TiVN-0.19	4.50	22.01	11.19	51.78	6.02	4.51	0.19	0.19
TiVN-0.55	8.90	15.00	11.60	53.14	6.03	5.33	0.56	0.55
TiVN-1.46	14.02	8.91	9.60	55.6 1	5.94	5.95	1.48	1.46

presence of larger amounts of titanium oxide or vanadium oxide in the samples can be excluded as shown by the absence of reflection patterns corresponding to the respective oxides in the XRD measurements (Figure 6). On the other hand, an incorporation of oxygen inside the crystal structure cannot be excluded since for both compounds Ti(ON)[37,38] and V(ON)[39] phases are known and inclusion of small amounts of oxygen should not change the XRD pattern significantly.

All three samples exhibit diffraction patterns with cubic symmetry and crystallize in the space group $Fm\bar{3}m$. The exact peak positions as well as the cell parameters are listed in Table 5. As observed for the Al−Ga−N nanoparticles, a shift in the diffraction angles is observed depending on the Ti/V molar ratio in the powders. Thus, with increasing vanadium content, the pattern shifts to higher angles, that is, from the pattern of pure TiN toward the pattern of pure VN, indicating the formation of a homogeneous Ti−V−N solid solution.

From the Scherer equation applied to the (200) and the (111) peak, an average crystallite size was determined for each sample. The crystallite size decreases from 5.0 to 3.7 nm with increasing vanadium content, indicated by a progressive broadening of the diffraction peaks. In contrast, the crystallite size of the two binary nitrides is similar at approximately 5 nm.

The shape and size of the particles were furthermore investigated by TEM measurements (Figure 7). The TEM images show small particles of narrow dispersity, which are, contrary to the Al−Ga−N particles, not isolated but embedded in an amorphous matrix, most probably formed from the residual carbon. The higher agglomeration and thus higher density of the particles enables additional confirmation of the crystallinity of the samples using selected area electron diffraction (SAED). The observed SAED patterns can be attributed to Ti−V−N alloys.

HRTEM measurements show that the particles are highly crystalline, and well-developed lattice fringes can be observed (Figure 8). From the corresponding FFT, the lattice distances were determined. However, particles with similar orientations were harder to find in these samples, making an accurate comparison of the lattice distances difficult. Moreover, the presence of residual carbon causes significant background noise in the FFT. Still a trend toward smaller lattice distances with increasing vanadium content is observed.

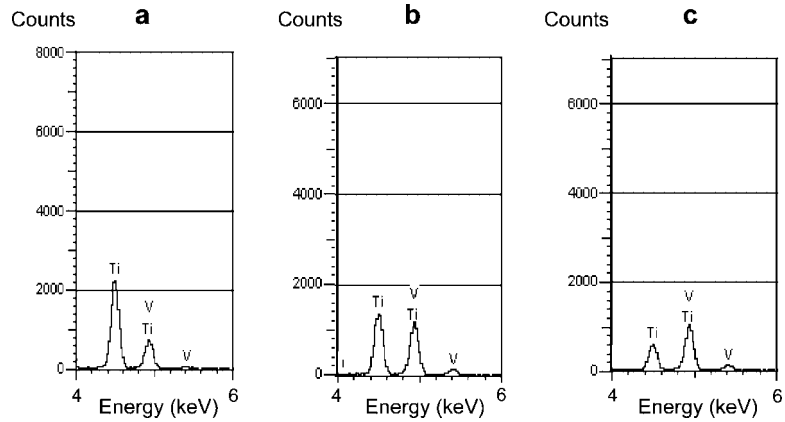

Figure 5. EDX measurements of the Ti−V−N nanoparticles: (a) TiVN-0.19, (b) TiVN-0.55, and (c) TiVN-1.46.

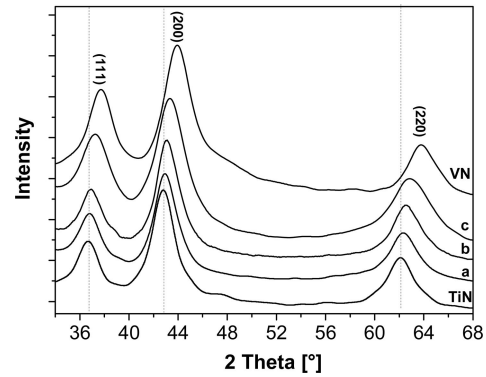

Figure 6. X-ray diffraction pattern of the Ti−V−N powders with increasing vanadium content: (a) TiVN-0.19, (b) TiVN-0.55, and (c) TiVN-1.46. As a reference, the patterns of pure TiN and VN synthesized in the same reaction conditions are shown.

TABLE 5. Diffraction Peak Positions, Cell Parameters, and Crystallite Size of the Observed Ti−V−N, TiN, and VN Powders Synthesized in the Same Reaction Conditions

	cell parameter [Å] $Fm\bar{3}m$		
sample	a = b = c	cryst size XRD	particle size TEM
TiN	4.233	4.8	5.6
TiVN-0.19	4.220	5.0	5.0
TiVN-0.55	4.205	4.6	5.0
TiVN-1.46	4.160	3.7	4.0
VN	4.130	4.9	5.5

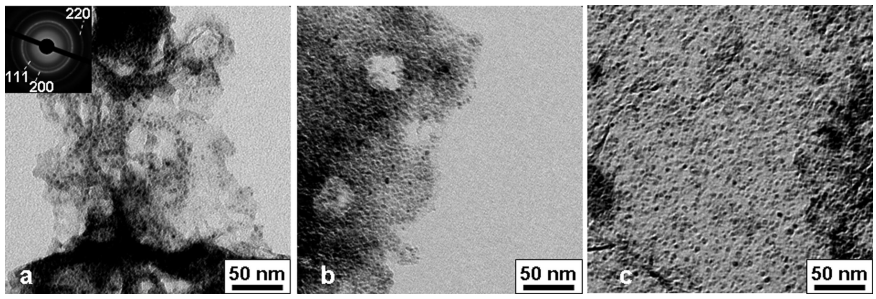

Figure 7. TEM micrographs and SAED of the Ti−V−N samples: (a) TiVN-0.19, (b) TiVN-0.55, and (c) TiVN-1.46.

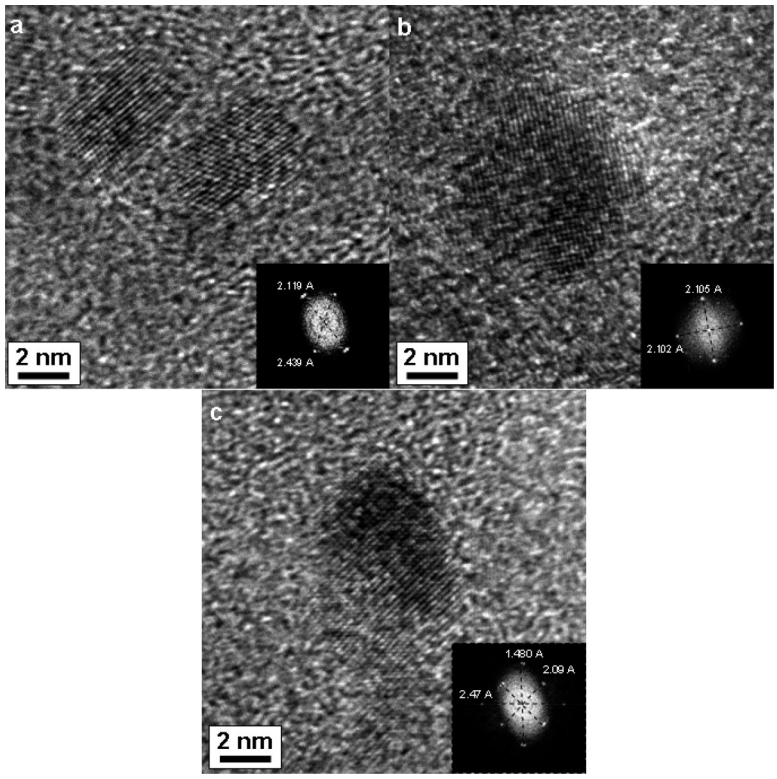

Figure 8. HRTEM micrographs and FFT spectrum of the Ti−V−N samples: (a) TiVN-0.19, (b) TiVN-0.55, and (c) TiVN-1.46.

CONCLUSION

In conclusion, mesoporous graphitic carbon nitride (mpg-C_3N_4) was used as a "reactive template" for the synthesis of ternary metal nitride nanoparticles. Infiltration of solutions of mixed precursors and removal of the solvent yield the formation of mixed metal oxide nanoparticles in the pores. Subsequent heating under inert gas yields decomposition of the metal nitride and the donation of nitrogen atoms to the preformed oxide nanoparticles. Thus, in the first step, mpg-C_3N_4 acts as a classical exotemplate, while in the second step, it acts as reactant for the conversion of the oxide into the nitride. Using this approach, ternary metal nitride nanoparticles with particle sizes smaller than 10 nm, narrow dispersities, and controlled composition could be synthesized, here exemplified by the synthesis of Al−Ga−N and Ti−V−N nanoparticles, respectively.

EDX measurements revealed that the composition of the final nitrides is simply dependent on the prior used precursor ratios, while XRD and HRTEM proved that indeed homogeneous, solid solutions of the two metal nitrides have formed also on the scale of one single nanoparticle. From these examples, it can be assumed that the reactive templating shown here is a quite general approach, which could be used for the preparation of nanoparticles with a wide variety of other ternary metal nitride compositions. Furthermore, as the nanoconfinement prevents any phase separation or demixing of the metals, there seems to be no borderline to the used metal compositions, and even the generation of quaternary and higher metal nitrides can be envisaged. Also, as the size of the nanoparticles can be tuned by simply changing the concentration of the preceding solutions,[32] not only the composition but also the size of the nanoparticles should be easily adjustable. Thus we think that the reactive templating shown here can certainly complement other metal nitride syntheses, such as post-treatment of mixed oxides with nitrogen donors such as ammonia.

Nanoparticles are presumably the most often described nanostructure of inorganic materials. However, it should be noted that for this conceptual paper we restricted ourselves to the simplest topology of the reactive template, a mesoporous carbon nitride with spherical pores produced by templating silica nanoparticles. The ternary metal nitride particles produced here are therefore in the end just a direct copy of the morphology of the initially used silica nanoparticles. Considering the abundance of other silica nanostructures available, from particles to porous materials, a variety of other morphologies in which ternary metal nitrides can be shaped can be envisaged using the approach shown here.

METHODS

All chemicals were used as received without any further purification.

Synthesis of Mesoporous C_3N_4. The nanoreactor, mpg-C_3N_4, was synthesized as previously described.[33] In a typical synthesis, 2.5 g of a 40 wt % aqueous silica nanoparticle solution (Ludox HS40, Ø ~ 12 nm, Aldrich) was added to 1 g of molten cyanamide (CH_2N_2, Aldrich). The mixture was then heated to 90 °C under vigorous stirring to ensure the slow evaporation of the water. The resulting white solid was heated in a closed ceramic crucible to 550 °C for 4 h. Removal of the silica nanoparticles with

a 4 M NH_4HF_2 solution yielded mesoporous graphitic carbon nitride (mpg-C_3N_4). Caution is advised as NH_4HF_2 causes severe burns in contact with skin.

Synthesis of Metal Nitride Alloy Nanoparticles A—B—N. In a general synthesis, the respective amount of precursors A and B was dissolved in 2.0 g of ethanol. Caution is advised because the described metal precursors ($GaCl_3$, $AlCl_3$, $TiCl_4$, and $VOCl_3$) react vigorously with ethanol. Transparent solutions were obtained in all cases. The exact composition of the used precursor solutions is given in Table 1.

To these solutions was added 0.5 g of mesoporous g-C_3N_4. The mixtures were sonicated for 10 min and placed shortly under reduced pressure to free the pores from air and thus to achieve a good penetration of the solution inside the pores. The infiltrated mesoporous powder was collected by suction filtration washed dropwise under suction with 2 mL of EtOH, and finally dried on the filter. The resulting powder was heated to 800 °C for 4 h and kept there for 3 h, both under a flow of nitrogen. ***Caution is advised*** as the thermal decomposition of C_3N_4 can yield the production of toxic gases such as HCN. Thus, ovens have to be placed in a fume hood or places with sufficient ventilation.

After the heat treatment, light brown to gray powders for Al—Ga—N and black powders for Ti—V—N were obtained, respectively.

Characterization. TEM images were taken on a Zeiss EM Omega 912X at an acceleration voltage of 120 kV. The as-made powders were grinded and dispersed in acetone or THF. One droplet of oleic acid was added, and the suspension was strongly sonicated several times with a high power sonicating tip to ensure better dispersion of the particles. One droplet of the suspension was applied to a 400 mesh carbon-coated copper grid and left to dry. HRTEM images of the Al—Ga—N particles were performed on a Phillips TEM/STEM CM 200 FEG transmission electron microscope equipped with a field-emission gun operated at 200 kV. HRTEM images of the Ti—V—N samples were conducted with a JEOL TEM/STEM JEM-2100F-UHR transmission electron microscope equipped with a field-emission gun operated at 200 kV.

XRD measurements were carried out in reflection mode on a Bruker D8 diffractometer. The emitted Cu Kα radiation (λ = 0.154 nm) was monochromated by a multilayer Göbel mirror. An energy dispersive detector (Sol-X, Bruker) was used to ensure low background noise, by filtering out the inelastic scattered photons. SEM measurements were carried out on a DSM 940 A microscope from Zeiss (Oberkochen), which operates at 20 kV. For EDX measurements, a Link-ISIS 300 from Oxford Instruments (UK) was used. Elemental analyses were performed with a VARIO EL elemental analysis instrument to determine the carbon, nitrogen, hydrogen, and sulfur content of the samples.

Acknowledgment. Financial support by the Max Planck Society within the framework of the project ENERCHEM is gratefully acknowledged.

Supporting Information Available: Analysis (XRD, TEM, SAXS, BET) of the reactive template, mpg-C_3N_4, diffraction peak positions of the Al—Ga—N and Ti—V—N, and additional HRTEM micrographs for Al—Ga—N nanoparticles are reported. This material is available free of charge *via* the Internet at http://pubs.acs.org.

REFERENCES AND NOTES

1. Sirvio, E. H.; Sulonen, M.; Sundquist, H. Abrasive Wear of Ion-Plated Titanium Nitride Coatings on Plasma-Nitrided Steel Surfaces. *Thin Solid Films* **1982**, *96*, 93–101.
2. Ponce, F. A.; Bour, D. P. Nitride-Based Semiconductors for Blue and Green Light-Emitting Devices. *Nature* **1997**, *386*, 351–359.
3. Choi, D.; Blomgren, G. E.; Kumta, P. N. Fast and Reversible Surface Redox Reaction in Nanocrystalline Vanadium Nitride Supercapacitors. *Adv. Mater.* **2006**, *18*, 1178–1182.
4. Krawiec, P.; De Cola, P. L.; Glaser, R.; Weitkamp, J.; Weidenthaler, C.; Kaskel, S. Oxide Foams for the Synthesis of High-Surface-Area Vanadium Nitride Catalysts. *Adv. Mater.* **2006**, *18*, 505–508.
5. Kaskel, S.; Schlichte, K.; Kratzke, T. Catalytic Properties of High Surface Area Titanium Nitride Materials. *J. Mol. Catal. A: Chem.* **2004**, *208*, 291–298.
6. Kwon, H.; Choi, S.; Thompson, L. T. Vanadium Nitride Catalysts: Synthesis and Evaluation for *n*-Butane Dehydrogenation. *J. Catal.* **1999**, *184*, 236–246.
7. Ramanathan, S.; Oyama, S. T. New Catalysts for Hydroprocessing—Transition-Metal Carbides and Nitrides. *J. Phys. Chem.* **1995**, *99*, 16365–16372.
8. Fischer, A.; Makowski, P.; Müller, J. O.; Antonietti, M.; Thomas, A.; Goettmann, F. High-Surface-Area TiO_2 and TiN as Catalysts for the C—C Coupling of Alcohols and Ketones. *ChemSusChem* **2008**, *1*, 444–449.
9. Jain, S. C.; Willander, M.; Narayan, J.; Van Overstraeten, R. III-Nitrides: Growth, Characterization, and Properties. *J. Appl. Phys.* **2000**, *87*, 965–1006.
10. Benaissa, M.; Gonsalves, K. E.; Rangarajan, S. P. AlGaN Nanoparticle/Polymer Composite: Synthesis, Optical, and Structural Characterization. *Appl. Phys. Lett.* **1997**, *71*, 3685–3687.
11. Latella, B. A.; Gan, B. K.; Daviesb, K. E.; McKenzie, D. R.; McCulloch, D. G. Titanium Nitride/Vanadium Nitride Alloy Coatings: Mechanical Properties and Adhesion Characteristics. *Surf. Coat. Technol.* **2006**, *200*, 3605–3611.
12. Ichimiya, N.; Onishi, Y.; Tanaka, Y. Properties and Cutting Performance of (Ti,V)N Coatings Prepared by Cathodic Arc Ion Plating. *Surf. Coat. Technol.* **2005**, *200*, 1377–1382.
13. Choi, D.; Kumta, P. N. Nanocrystalline TiN Derived by a Two-Step Halide Approach for Electrochemical Capacitors. *J. Electrochem. Soc.* **2006**, *153*, A2298–A2303.
14. Herle, P. S.; Vasanthacharya, N. Y.; Hegde, M. S.; Gopalakrishnan, J. Synthesis of New Transition-Metal Nitrides, MWN2 (M = Mn, Co, Ni). *J. Alloys Compd.* **1995**, *217*, 22–24.
15. Bem, D. S.; Loye, H. C. Z. Synthesis of the New Ternary Transition-Metal Nitride FeWN2 *via* Ammonolysis of a Solid State Precursor. *J. Solid State Chem.* **1993**, *104*, 467–469.
16. Gomathi, A. Ternary Metal Nitrides by the Urea Route. *Mater. Res. Bull.* **2007**, *42*, 870–874.
17. Parkin, I. P. Solid State Metathesis Reaction for Metal Borides, Silicides, Pnictides and Chalcogenides: Ionic or Elemental Pathways. *Chem. Soc. Rev.* **1996**, *25*, 199–207.
18. Parkin, I. P.; Nartowski, A. M. Solid State Metathesis Routes to Group IIIa Nitrides: Comparison of Li_3N, NaN_3, Ca_3N_2 and Mg_3N_2 as Nitriding Agents. *Polyhedron* **1998**, *17*, 2617–2622.
19. Cumberland, R. W.; Blair, R. G.; Wallace, C. H.; Reynolds, T. K.; Kaner, R. B. Thermal Control of Metathesis Reactions Producing GaN and InN. *J. Phys. Chem. B* **2001**, *105*, 11922–11927.
20. Gillan, E. G.; Kaner, R. B. Rapid Solid-State Synthesis of Refractory Nitrides. *Inorg. Chem.* **1994**, *33*, 5693–5700.
21. Song, B.; Jian, J. K.; Wang, G.; Lei, M.; Xu, Y. P.; Chen, X. L. Facile and General Route to Nitrides by a Modified Solid-State Metathesis Pathway. *Chem. Mater.* **2007**, *19*, 1497–1502.
22. Hsu, C. W.; Ganguly, A.; Liang, C. H.; Hung, Y. T.; Wu, C. T.; Hsu, G. M.; Chen, Y. F.; Chen, C. C.; Chen, K. H.; Chen, L. C. Enhanced Emission of (In, Ga) Nitride Nanowires Embedded with Self-Assembled Quantum Dots. *Adv. Funct. Mater.* **2008**, *18*, 938–942.
23. Cai, X. M.; Leung, Y. H.; Cheung, K. Y.; Tam, K. H.; Djurisic, A. B.; Xie, M. H.; Chen, H. Y.; Gwo, S. Straight and Helical InGaN Core-Shell Nanowires with a High In Core Content. *Nanotechnology* **2006**, *17*, 2330–2333.
24. He, M. Q.; Mohammad, S. N. Novel Chemical-Vapor Deposition Technique for the Synthesis of High-Quality Single-Crystal Nanowires and Nanotubes. *J. Chem. Phys.* **2006**, *124*, 064714-1–064714-7.
25. Bhat, S. V.; Biswas, K.; Rao, C. N. R. Synthesis and Optical Properties of In-Doped GaN Nanocrystals. *Solid State Commun.* **2007**, *141*, 325–328.

26. Schwenzer, B.; Meier, C.; Masala, O.; Seshadri, R.; DenBaars, S. P.; Mishra, U. K. Synthesis of Luminescing (In, Ga)N Nanoparticles from an Inorganic Ammonium Fluoride Precursor. *J. Mater. Chem.* **2005**, *15*, 1891–1895.
27. Krawiec, P.; Panda, R. N.; Kockrick, E.; Geiger, D.; Kaskel, S. High Surface Area V-Mo-N Materials Synthesized from Amine Intercalated Foams. *J. Solid State Chem.* **2008**, *181*, 935–942.
28. Schuth, F. Endo- and Exotemplating to Create High-Surface-Area Inorganic Materials. *Angew. Chem., Int. Ed.* **2003**, *42*, 3604–3622.
29. Lu, A. H.; Schuth, F. Nanocasting: A Versatile Strategy for Creating Nanostructured Porous Materials. *Adv. Mater.* **2006**, *18*, 1793–1805.
30. Thomas, A.; Goettmann, F.; Antonietti, M. Hard Templates for Soft Materials: Creating Nanostructured Organic Materials. *Chem. Mater.* **2008**, *20*, 738–755.
31. Tiemann, M. Repeated Templating. *Chem. Mater.* **2008**, *20*, 961–971.
32. Fischer, A.; Antonietti, M.; Thomas, A. Growth Confined by the Nitrogen Source: Synthesis of Pure Metal Nitride Nanoparticles in Mesoporous Graphitic Carbon Nitride. *Adv. Mater.* **2007**, *19*, 264–267.
33. Goettmann, F.; Fischer, A.; Antonietti, M.; Thomas, A. Chemical Synthesis of Mesoporous Carbon Nitrides Using Hard Templates and Their Use as a Metal-Free Catalyst for Friedel−Crafts Reaction of Benzene. *Angew. Chem., Int. Ed.* **2006**, *45*, 4467–4471.
34. Thomas, A.; Fischer, A.; Goettmann, F.; Antonietti, M.; Muller, J.-O.; Schlogl, R.; Carlsson, J. M. Graphitic Carbon Nitride Materials: Variation of Structure and Morphology and Their Use as Metal-Free Catalysts. *J. Mater. Chem.* **2008**, *18*, 4893–4908.
35. Stutzmann, M.; Ambacher, O.; Cros, A.; Brandt, M. S.; Angerer, H.; Dimitrov, R.; Reinacher, N.; Metzger, T.; Hopler, R.; Brunner, D.; et al. Properties and Applications of MBE Grown AlGaN. *Mater. Sci. Eng., B* **1997**, *50*, 212–218.
36. Buha, J.; Djerdj, I.; Antonietti, M.; Niederberger, M. Thermal Transformation of Metal Oxide Nanoparticles into Nanocrystalline Metal Nitrides Using Cyanamide and Urea as Nitrogen Source. *Chem. Mater.* **2007**, *19*, 3499–3505.
37. Hitoki, G.; Takata, T.; Kondo, J. N.; Hara, M.; Kobayashi, H.; Domen, K. (Oxy)nitrides as New Photocatalysts for Water Splitting under Visible Light Irradiation. *Electrochemistry* **2002**, *70*, 463–465.
38. Martinez-Ferrero, E.; Sakatani, Y.; Boissiere, C.; Grosso, D.; Fuertes, A.; Fraxedas, J.; Sanchez, C. Nanostructured Titanium Oxynitride Porous Thin Films as Efficient Visible-Active Photocatalysts. *Adv. Funct. Mater.* **2007**, *17*, 3348–3354.
39. Parkin, I. P.; Elwin, G. S. Atmospheric Pressure Chemical Vapour Deposition of Vanadium Nitride and Oxynitride Films on Glass from Reaction of VCl_4 with NH_3. *J. Mater. Chem.* **2001**, *11*, 3120–3124.